

Article

Encapsulation of Upconversion Nanoparticles in Periodic Mesoporous Organosilicas

Saher Rahmani ¹, Chiara Mauriello Jimenez ¹, Dina Aggad ², Daniel González-Mancebo ³, Manuel Ocaña ³, Lamiaa M. A. Ali ², Christophe Nguyen ², Ana Isabel Becerro Nieto ³ , Nadège Francolon ⁴, Erwan Oliveiro ¹, Damien Boyer ⁴ , Rachid Mahiou ⁴ , Laurence Raehm ¹, Magali Gary-Bobo ², Jean-Olivier Durand ¹  and Clarence Charnay ^{1,*} 

¹ Institut Charles Gerhardt Montpellier, case 1701, UMR5253, CNRS-UM-ENSCM, Place Eugène Bataillon, 34095 Montpellier, CEDEX 05, France; rahmeni.sahar@yahoo.fr (S.R.); chiaramauriellojimenez@gmail.com (C.M.J.); erwan.oliveiro@umontpellier.fr (E.O.); laurence.raehm@umontpellier.fr (L.R.); durand@univ-montp2.fr (J.-O.D.)

² Institut des Biomolécules Max Mousseron UMR 5247 CNRS, UM-Faculté de Pharmacie, 15 Avenue Charles Flahault, 34093 Montpellier, CEDEX 05, France; dina.aggad@gmail.com (D.A.); lamiaa.ali@umontpellier.fr (L.M.A.A.); christophe.nguyen@umontpellier.fr (C.N.); magali.gary-bobo@inserm.fr (M.G.-B.)

³ Instituto de Ciencia de Materiales de Sevilla (CSIC-US), c/Américo Vespucio, 49, 41092 Seville, Spain; dagoman_89@hotmail.com (D.G.-M.); mjurado@icmse.csic.es (M.O.); anieto@icmse.csic.es (A.I.B.N.)

⁴ Université Clermont Auvergne, CNRS, SIGMA Clermont, ICCF, F-63000 Clermont-Ferrand, France; francolon.nadege@hotmail.fr (N.F.); damien.boyer@sigma-clermont.fr (D.B.); rachid.mahiou@uca.fr (R.M.)

* Correspondence: clarence.charnay@umontpellier.fr; Tel.: +3-34-6714-3864

Received: 30 September 2019; Accepted: 31 October 2019; Published: 9 November 2019



Abstract: (1) Background: Nanomedicine has recently emerged as a promising field, particularly for cancer theranostics. In this context, nanoparticles designed for imaging and therapeutic applications are of interest. We, therefore, studied the encapsulation of upconverting nanoparticles in mesoporous organosilica nanoparticles. Indeed, mesoporous organosilica nanoparticles have been shown to be very efficient for drug delivery, and upconverting nanoparticles are interesting for near-infrared and X-ray computed tomography imaging, depending on the matrix used. (2) Methods: Two different upconverting-based nanoparticles were synthesized with $\text{Yb}^{3+}\text{-Er}^{3+}$ as the upconverting system and NaYF_4 or BaLuF_5 as the matrix. The encapsulation of these nanoparticles was studied through the sol-gel procedure with bis(triethoxysilyl)ethylene and bis(triethoxysilyl)ethane in the presence of CTAB. (3) Results: with bis(triethoxysilyl)ethylene, $\text{BaLuF}_5\text{: Yb}^{3+}\text{-Er}^{3+}$, nanoparticles were not encapsulated, but anchored on the surface of the obtained mesoporous nanorods $\text{BaLuF}_5\text{: Yb}^{3+}\text{-Er}^{3+}\text{@Ethylene}$. With bis(triethoxysilyl)ethane, $\text{BaLuF}_5\text{: Yb}^{3+}\text{-Er}^{3+}$ and $\text{NaYF}_4\text{: Yb}^{3+}\text{-Er}^{3+}$ nanoparticles were encapsulated in the mesoporous cubic structure leading to $\text{BaLuF}_5\text{: Yb}^{3+}\text{-Er}^{3+}\text{@Ethane}$ and $\text{NaYF}_4\text{: Yb}^{3+}\text{-Er}^{3+}\text{@Ethane}$, respectively. (4) Conclusions: upconversion nanoparticles were located on the surface of mesoporous nanorods obtained by hydrolysis polycondensation of bis(triethoxysilyl)ethylene, whereas encapsulation occurred with bis(triethoxysilyl)ethane. The later nanoparticles $\text{NaYF}_4\text{: Yb}^{3+}\text{-Er}^{3+}\text{@Ethane}$ or $\text{BaLuF}_5\text{: Yb}^{3+}\text{-Er}^{3+}\text{@Ethane}$ were promising for applications with cancer cell imaging or X-ray-computed tomography respectively.

Keywords: upconversion; periodic mesoporous organosilica nanoparticles; cancer

1. Introduction

Periodic mesoporous organosilica nanoparticles (PMON) have gained increasing attention for nanomedicine applications [1–3]. These nanoparticles are prepared from trialkoxypolysilylated organic

precursors without the presence of any silica sources. The properties of these nanoparticles are very different from those of Mesoporous Silica Nanoparticles (MSN), which are at the forefront of bio-applications [4–7]. Indeed, PMON present higher loading capacities of hydrophilic and hydrophobic molecules than MSN due to the interaction with the organic matrix, and are less hemolytic than MSN as well as being biocompatible [8,9]. Degradability of PMON can be triggered by glutathione by introducing disulfide bridges in the matrix [10]. Core-shell systems have also been described with iron oxide [11], gold [12,13], or nanodiamonds [14] as the core. In the course of our work on PMON, we were interested in systems for theranostic applications with upconversion nanoparticles as their core, capable of being imaged by infrared or X-ray excitations. Indeed, upconversion nanoparticles present attractive features [15] such as near-infrared excitation at low power with deep penetration in living tissues, and biocompatibility in vivo when stabilized with dendrimers [16], or a mesoporous silica shell [17,18]. The matrix is usually NaYF₄, but using Lu³⁺ instead of Y³⁺ endows the nanoparticles with X-ray sensitivity [19,20]. In the present work, we studied the encapsulation of upconversion NaYF₄: Yb³⁺-Er³⁺ or BaLuF₅: Yb³⁺-Er³⁺ nanoparticles with bis(triethoxysilyl)ethylene or bis(triethoxysilyl)ethane as the PMO precursors. We showed that no encapsulation occurred with BaLuF₅: Yb³⁺-Er³⁺ and bis(triethoxysilyl)ethylene. BaLuF₅: Yb³⁺-Er³⁺ nanoparticles were anchored on the surface of BaLuF₅: Yb³⁺-Er³⁺@Ethylene mesoporous nanorods, whereas core-shell systems were observed with bis(triethoxysilyl)ethane. We obtained core-shell nanoparticles with NaYF₄: Yb³⁺-Er³⁺ or BaLuF₅: Yb³⁺-Er³⁺ as core. NaYF₄: Yb³⁺-Er³⁺@Ethane nanoparticles were incubated with MCF-7 breast cancer cells and excitation in the NIR at 980 nm with a two-photon microscope made it possible to observe endocytosis of the nanoparticles. Alternatively, BaLuF₅: Yb³⁺-Er³⁺@Ethane nanoparticles showed X-ray absorption properties when irradiated. Ethane-based PMON are, therefore, promising for theranostics applications.

2. Results and Discussion

For the synthesis of Yb³⁺-Er³⁺, BaLuF₅@Ethylene, the sol-gel procedure was carried out in highly diluted conditions. First, CTAB was dissolved in water with NaOH and after the formation of micelles, BaLuF₅: Yb³⁺-Er³⁺ nanoparticles were added in order to encapsulate the nanoparticles inside the micelles. Thirty minutes later, bis(triethoxysilyl)ethylene in EtOH was added and the mixture reacted for two hours. BaLuF₅: Yb³⁺-Er³⁺@Ethylene nanoparticles were then centrifuged and the surfactant extracted with a solution of ammonium nitrate in 95% EtOH. The SEM and TEM of Yb³⁺-Er³⁺, BaLuF₅@Ethylene nanoparticles are displayed in Figure 1A,B respectively. We observed 400 nm length and 150 nm width mesoporous nanorods as expected [21].

Surprisingly, the upconversion BaLuF₅: Yb³⁺-Er³⁺ nanoparticles were not embedded inside the structure, but were located on the surface, on the top of the nanorod, as clearly shown by SEM and TEM. The mesoporous structure was shown by N₂ sorption experiments, with a BET surface of more than 1000 m²g⁻¹ and small pores of 2.5 nm (Figure 1C). EDX confirmed the presence of characteristic elements of the inorganic matrix (Yb, Lu, Ba, and F).

We then examined the hydrolysis-polycondensation of bis(triethoxysilyl)ethane in the presence of NaYF₄: Yb³⁺-Er³⁺ or BaLuF₅: Yb³⁺-Er³⁺ nanoparticles, using essentially the same procedure as above. Note that bis(triethoxysilyl)ethane was not diluted in EtOH before its addition to the reaction. With NaYF₄: Yb³⁺-Er³⁺, we obtained monodisperse 543 nm-diameter nanoparticles after reaction and extraction of the surfactant, as shown by TEM (Figure 2A) and dynamic light scattering (DLS) in EtOH, which displayed diameters centered at 543 nm showing the monodispersity of the system (Figure 2D). Magnification displayed core-shell systems with NaYF₄: Yb³⁺-Er³⁺ as the core and a mesoporous organosilica shell (Figure 2B). The core was still luminescent after encapsulation as shown in Figure 2C. After excitation at 980 nm, green (550 nm) and red (670 nm) luminescence was detected.

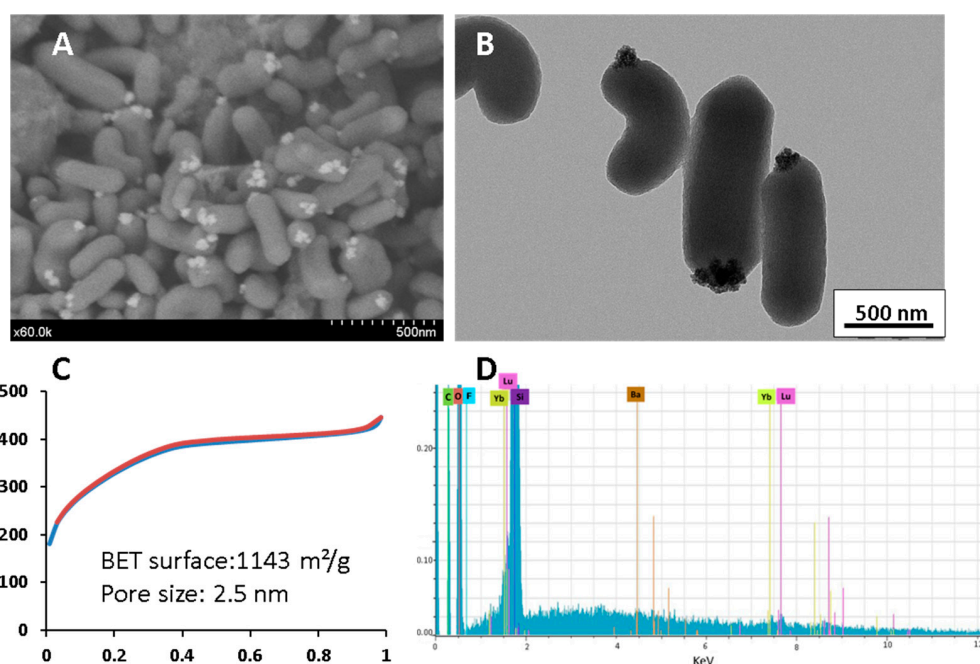


Figure 1. (A) SEM image of BaLuF₅: Yb³⁺-Er³⁺@Ethylene (B) TEM of BaLuF₅: Yb³⁺-Er³⁺@Ethylene, scale bar 500 nm. (C) N₂ adsorption–desorption experiment of Yb³⁺-Er³⁺, BaLuF₅ @Ethylene (D) EDX analysis of BaLuF₅: Yb³⁺-Er³⁺@Ethylene. C, O, F, Yb, Lu, Si, Ba, Yb, Lu elements were detected.

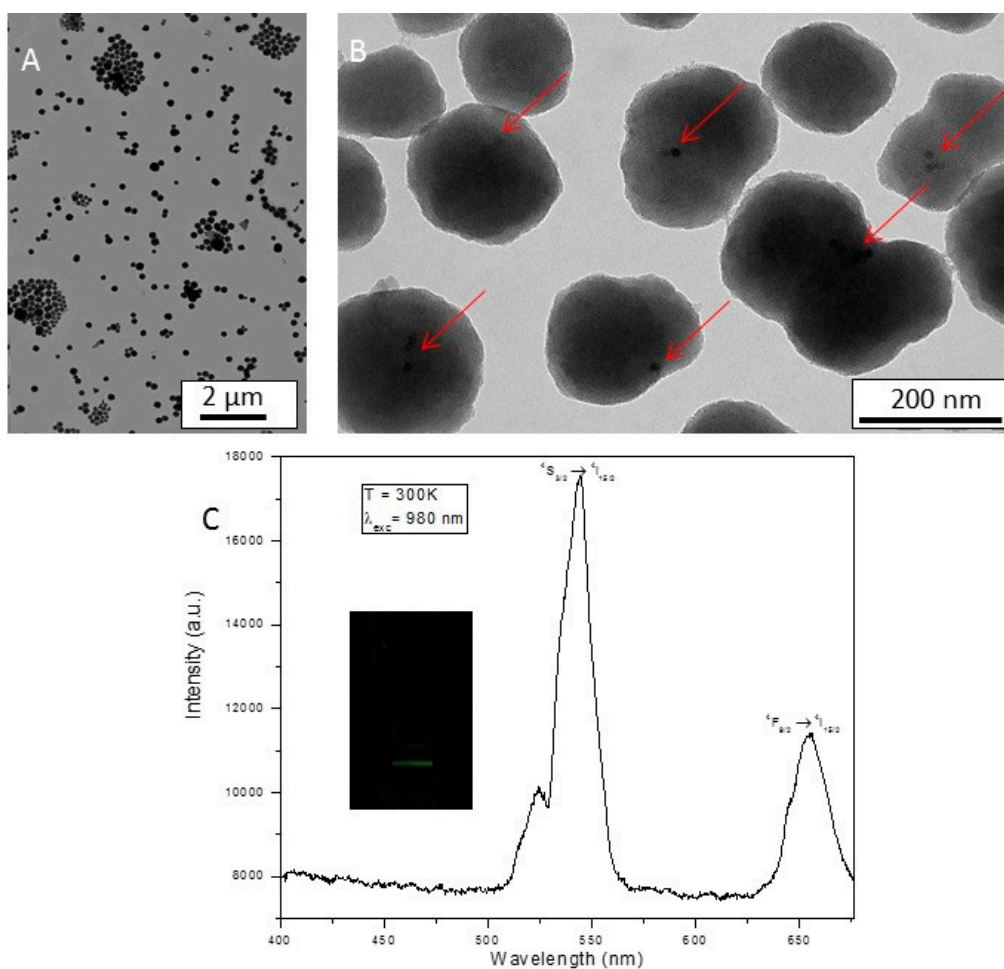


Figure 2. Cont.

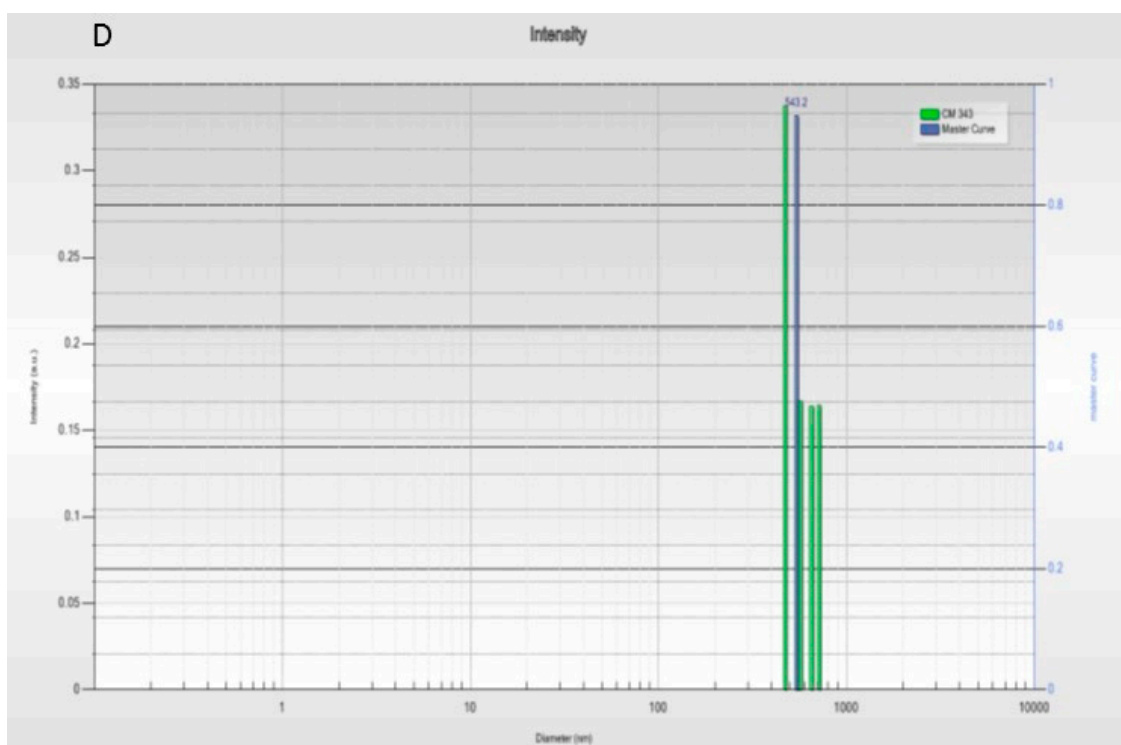


Figure 2. (A) TEM image of NaYF₄: Yb³⁺-Er³⁺@Ethane scale bar 2 μm . (B) TEM of NaYF₄: Yb³⁺-Er³⁺@Ethane, scale bar 200 nm. Red arrows show the embedded upconversion nanoparticles. (C) Luminescence spectrum of NaYF₄: Yb³⁺-Er³⁺@Ethane upon excitation at 973 nm (D) DLS of NaYF₄: Yb³⁺-Er³⁺@Ethane, in EtOH.

We then decided to investigate the imaging potential of NaYF₄: Yb³⁺-Er³⁺@Ethane and to study their cytotoxicity on cancer cells in culture. Cytotoxicity data in MCF-7 cells after 3 days of incubation with different concentrations of NaYF₄: Yb³⁺-Er³⁺@Ethane showed the classical sigmoidal dose-response curves when plotted as a logarithmic function of nanoparticles concentration ($\mu\text{g mL}^{-1}$) as shown in Figure 3A. The mean lethal concentration (LC₅₀) value was 51.56 $\mu\text{g mL}^{-1}$. NaYF₄: Yb³⁺-Er³⁺@Ethane nanoparticles (50 $\mu\text{g mL}^{-1}$) were then incubated with MCF-7 cancer cells, for 24 h. Fifteen minutes before the imaging experiment, the membranes of the cells were stained with a cell mask, and the cells were then imaged with a two-photon microscope at 980 nm. Figure 3B clearly demonstrated that NaYF₄: Yb³⁺-Er³⁺@Ethane nanoparticles were endocytosed by MCF-7 cancer cells, as the luminescence of the system was detected inside the cells. In addition, the percentage of labeled cells (Figure 3C) with nanoparticles was determined using the ImageJ program on 9 pictures for each concentration. For a 25 $\mu\text{g mL}^{-1}$ concentration, 46 \pm 12% of cells were labeled with nanoparticles. Meanwhile, at a 50 $\mu\text{g mL}^{-1}$ concentration, 58 \pm 8% of cells were labeled with nanoparticles.

With BaLuF₅: Yb³⁺-Er³⁺ nanoparticles, monodisperse core-shell systems were obtained with a size of 393 nm for BaLuF₅: Yb³⁺-Er³⁺@Ethane as shown by TEM (Figure 4A). Moreover, Figure 4D shows monodisperse nanoparticles with diameters centered at 393 nm as displayed by DLS in EtOH. HRTEM revealed a mesoporous structure with a classical cubic arrangement of mesopores (Figure 4B) [22]. The BaLuF₅: Yb³⁺-Er³⁺ cores were wrapped with the periodic mesoporous organosilica shell. The presence of silicon, barium, lutetium, and fluoride elements are confirmed as observed on the displayed spectra (Figure 4E). Moreover, these nanoparticles were able to absorb X-ray, as shown by X-ray computed tomography (Figure 4C). Indeed, the nanoparticles were placed in a plastic tube as a powder. The presence of the Lu atom led to X-ray absorption of BaLuF₅: Yb³⁺-Er³⁺@Ethane with a good contrast observed as already seen with bare Lu-based nanospheres [19]. BaLuF₅: Yb³⁺-Er³⁺@Ethane could thus be used as contrast agents for X-ray CT.

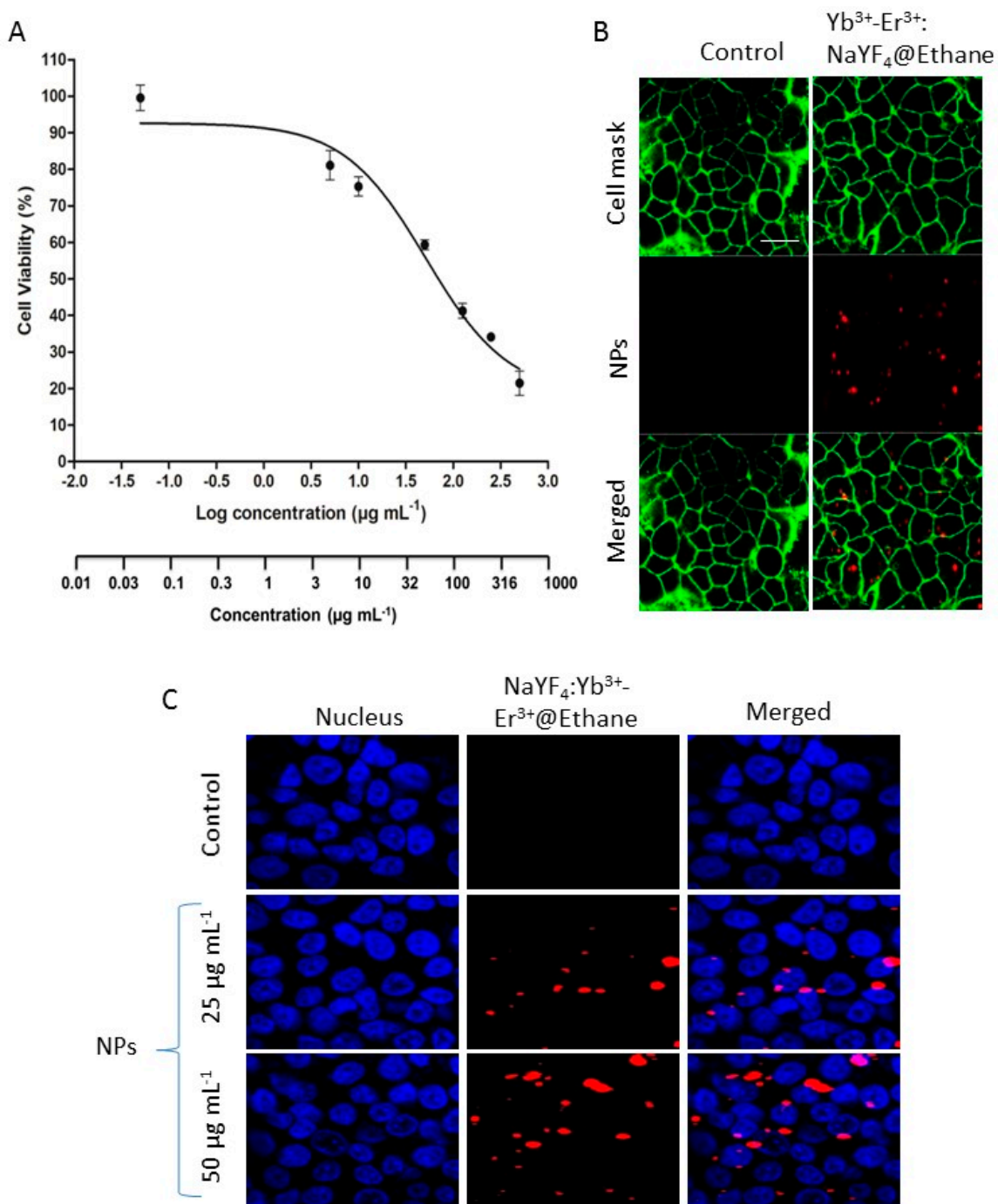


Figure 3. (A) Dose-response curve of MCF-7 cells treated with different concentrations of $\text{NaYF}_4\text{:Yb}^{3+}\text{-Er}^{3+}\text{@Ethane}$ for 3 days. Data are presented as mean \pm SEM ($n = 3$). (B) Near-Infrared Imaging at 980 nm of MCF-7 cells incubated with cell mask (green) and $\text{NaYF}_4\text{:Yb}^{3+}\text{-Er}^{3+}\text{@Ethane}$ (red dots) at $50 \mu\text{g mL}^{-1}$. (C) Near-Infrared Imaging at 980 nm of MCF-7 cells incubated with Hoechst 33,342 (blue) and $\text{NaYF}_4\text{:Yb}^{3+}\text{-Er}^{3+}\text{@Ethane}$ (red dots) at $25 \mu\text{g mL}^{-1}$ or $50 \mu\text{g mL}^{-1}$.

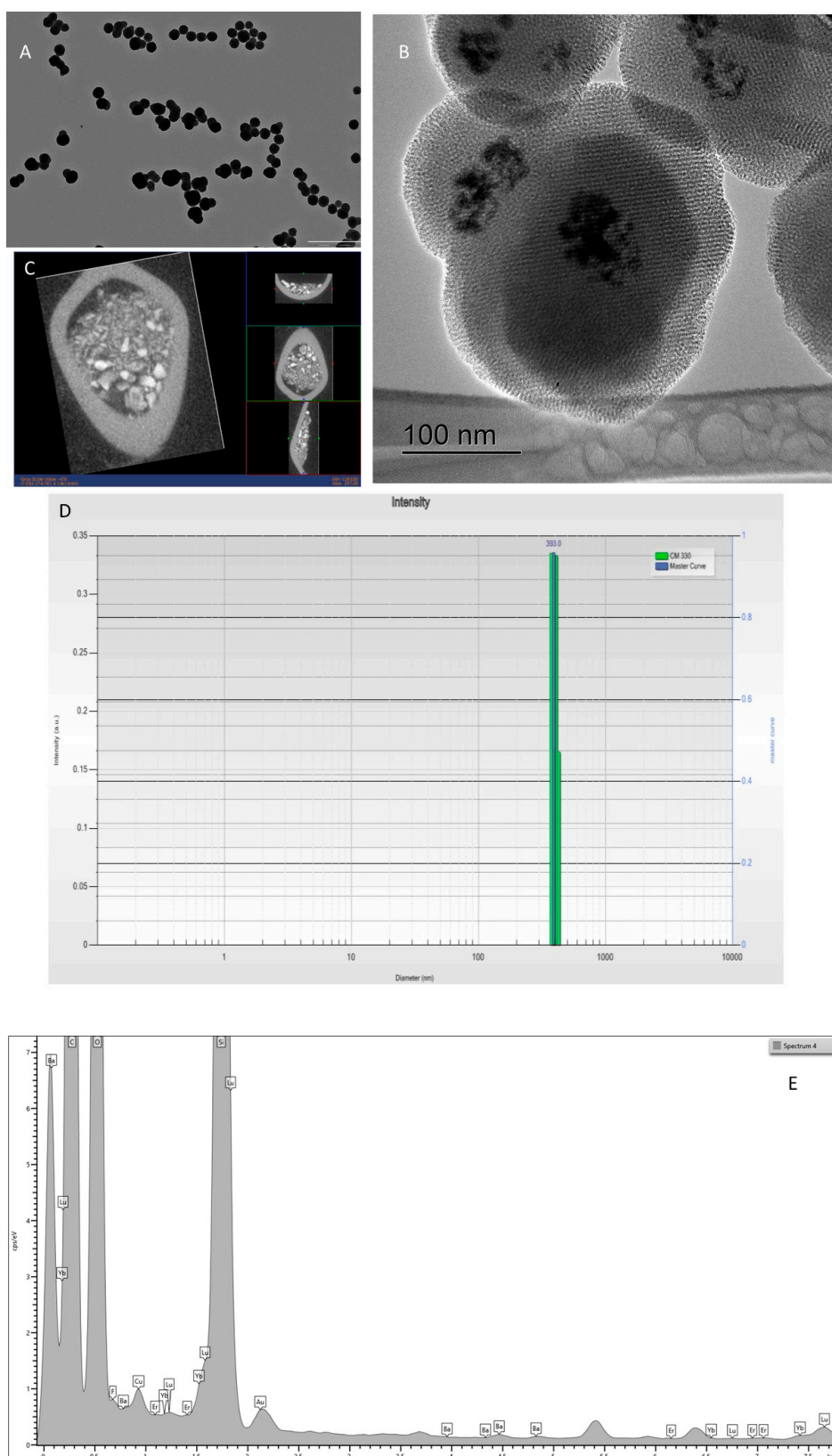


Figure 4. (A) TEM image of BaLuF₅: Yb³⁺-Er³⁺@Ethane scale bar 1 μ m (B) HRTEM of BaLuF₅: Yb³⁺-Er³⁺@Ethane. (C) X-ray computed tomography of BaLuF₅: Yb³⁺-Er³⁺@Ethane. (D) DLS of BaLuF₅: Yb³⁺-Er³⁺@Ethane in EtOH. (E) EDX analysis of BaLuF₅: Yb³⁺-Er³⁺@Ethane. Si, C, O, F, Ba, and Lu elements were detected.

3. Materials and Methods

Cetyltrimethylammonium bromide (CTAB), sodium hydroxide, ammonium nitrate (NH_4NO_3), and potassium bromide were purchased from Sigma-Aldrich. Absolute ethanol was purchased from Fisher Chemicals and hydrochloric acid from VWR PROLABO. Bis(triethoxysilyl)ethane and bis(triethoxysilyl)ethylene were purchased from ABCR (Karlsruhe, Germany).

Scanning electron microscope (SEM): Hitachi S4800 (Krefeld, Germany). The qualitative composition of the particles was assessed by energy dispersive X-ray analysis (EDX, EDX Bruker X Flash Detector 4010, Krefeld, Germany) coupled with the SEM microscope. TEM images were recorded with a JEOL 1200 EXII microscope (JEOL Europe SAS, Croissy Sur Seine, France) to visualize the shape of the NPs, HRTEM observation was performed with MET FEG JEOL 2200 FS, 200 kV (JEOL Europe SAS, Croissy Sur Seine, France). The element analysis on the observed core-shell nanoparticles (BaLuF_5 : Yb^{3+} - Er^{3+} @Ethane) was performed with DX TEM JEOL 1400 P+, 120 kV, and EDX SDD OXFORD. The presence of other elements such as copper or gold is due to the TEM grids and from the grid holder. For the purpose of TEM observations, the sample particles were dispersed in ethanol and then dropped onto copper grids with porous carbon films. The specific area and pore structure parameters of the studied NPs were determined from the measurements of nitrogen adsorption-desorption at 77 K with a TRISTAR 3000 Micromeritics using the Brunauer-Emmet-Teller (BET) method. For the sorption experiments, the samples (about 70 mg) were evacuated under vacuum at 80 °C for 12 h. DLS were recorded with a Vasco 135 Cordouan apparatus (Cordouan Technologies, Pessac, France).

Luminescence: The excitation is provided by a 980 nm beam of diode laser CNI Model FC-980 nm-4 W (cnilaser, Changchun, China). The UC emitted photons arising from NaYF_4 : Yb^{3+} , Er^{3+} @Ethane in ethanol are detected at room temperature at a right angle from the excitation and analyzed through a Jobin-Yvon monochromator (Triax 550, HORIBA Jobin Yvon, Palaiseau, France) combined with a cryogenically cold charge-coupled device (CCD) camera (Jobin-Yvon Symphony LN2 series, HORIBA Jobin Yvon, Palaiseau, France).

Synthesis of NaYF_4 :18% Yb^{3+} , 2% Er^{3+} nanoparticles: YCl_3 (0.8 mmol), YbCl_3 (0.18 mmol) and ErCl_3 (0.02 mmol) were dissolved in a mixture of 6 mL of oleic acid and 15 mL of octadecene (3/5 v/v). The solution was brought to 160 °C for 1 h to obtain a homogeneous mixture and the solution was cooled to room temperature. A second solution, containing 2.5 mmol of NaOH and 4 mmol of NH_4F previously dissolved in 10 mL of methanol, was added slowly to the previous mixture. The whole mixture was stirred for 30 min. and then heated at 100 °C for 10 min. Finally, the temperature was set at 320 °C for 1 h under argon flow. The solution was then cooled to room temperature and the nanocrystals were precipitated with ethanol. The nanocrystals were then washed with a cyclohexane/ethanol mixture (1/1 v/v) three times.

Synthesis of BaLuF_5 :20% Yb^{3+} -2% Er^{3+} nanoparticles: Appropriate amounts of barium nitrate ($\text{Ba}(\text{NO}_3)_2$), lutetium acetate hydrate ($(\text{CH}_3\text{CO}_2)_3\text{Lu}\cdot x\text{H}_2\text{O}$), ytterbium acetate hydrate ($(\text{CH}_3\text{CO}_2)_3\text{Yb}\cdot x\text{H}_2\text{O}$), and erbium acetate hydrate ($(\text{CH}_3\text{CO}_2)_3\text{Er}\cdot x\text{H}_2\text{O}$) were dissolved in 9.5 mL of ethylene glycol and admixed with 0.5 mL of 1-butyl-3-methylimidazolium tetrafluoroborate ([BMIM]BF₄). The resulting solution (final concentration of Ba = 0.01 M, Lu = 0.01 M, Yb = 2×10^{-3} M, Er = 2×10^{-5} M) was magnetically stirred for 5 min at room temperature to favor homogenization and aged for 15 h. in tightly closed test tubes using an oven preheated at 120 °C. After cooling down to room temperature, the suspension was centrifuged to remove supernatant and washed with ethanol and water.

Synthesis of BaLuF_5 : Yb^{3+} - Er^{3+} @Ethylene: CTAB (38.4 mg) and NaOH (1 M, 78 μL) were mixed in H_2O (120 mL), and heated at 80 °C at a stirring speed of 750 rpm. In a separate vial, BaLuF_5 : Yb^{3+} - Er^{3+} nanoparticles (1 mL) were diluted in H_2O (1 mL) and sonicated for 1 h. The BaLuF_4 nanoparticles were then added in the surfactant solution and stirred for 30 min. at 750 rpm. Bis(triethoxysilyl)ethylene (200 μL , 0.53 mmol) in 18 mL EtOH was then added to the solution and the reaction stirred at 80 °C for 2 h. The reaction was cooled to RT, then centrifuged (20 min, 20,000 rpm), and the surfactant was extracted with a solution of NH_4NO_3 (6g L⁻¹; EtOH 95%), by dispersing the nanoparticles at 40 °C

under ultrasound for 20 min followed by centrifugation. The procedure was repeated twice, and the nanoparticles washed with water and EtOH. The powder was dried at RT under vacuum.

Synthesis of BaLuF₅: Yb³⁺-Er³⁺@Ethane: CTAB (125 mg) and NaOH (2 M, 437 µL) were mixed in H₂O (60 mL), and heated at 80 °C at a stirring speed of 750 rpm. In a separate vial, BaLuF₅: Yb³⁺-Er³⁺ nanoparticles (1.5 mL) were diluted in H₂O (1 mL) and sonicated for 1 h. The BaLuF₅ nanoparticles were then added in the surfactant solution and stirred for 30 min. at 750 rpm. Bis(triethoxysilyl)ethane (184 µL, 0.49 mmol) was then added to the solution and the reaction stirred at 80 °C for 2 h. The reaction was cooled to RT, then centrifuged (20 min, 20,000 rpm), and the surfactant was extracted with a solution of NH₄NO₃ (6g L⁻¹; EtOH 95%), by dispersing the nanoparticles at 40 °C under ultrasounds for 20 min. and centrifugation. The procedure was repeated twice, and the nanoparticles washed with water and EtOH. The powder was dried at RT under vacuum.

Synthesis of NaYF₄: Yb³⁺-Er³⁺@Ethane: CTAB (125 mg), NaOH (2 M, 437 µL), were mixed in H₂O (60 mL), and heated at 80 °C at a stirring speed of 750 rpm. In a separate vial, NaYF₄: Yb³⁺-Er³⁺ nanoparticles (16 mg) were diluted in H₂O (2 mL) and sonicated for 1 h. The NaYF₄ nanoparticles were then added in the surfactant solution and stirred for 30 min at 750 rpm. Bis(triethoxysilyl)ethane (184 µL, 0.49 mmol) was then added to the solution and the reaction stirred at 80 °C for 2 h. The reaction was cooled to RT, then centrifuged (20 min, 20,000 rpm), and the surfactant was extracted with a solution of NH₄NO₃ (6g L⁻¹; EtOH 95%), by dispersing the nanoparticles at 40 °C under ultrasound for 20 min followed by centrifugation. The procedure was repeated twice, and the nanoparticles washed with water and EtOH. The powder was dried at RT under vacuum.

Cell culture: Human breast adenocarcinoma cell line (MCF-7) were maintained in Dulbecco's Modified Eagle Medium: Nutrient Mixture F-12 (DMEM/F12), which is a commercial medium widely used for the culture of mammalian cells and available in all consumable providers for cell biology. Additionally, 10% of fetal bovine serum was added for proteins, fatty acids, and growth factors. This medium was also supplemented with antibiotics (50 µg·mL⁻¹ gentamycin) to ensure cell safety. Finally, these cells were allowed to grow in a humidified atmosphere at 37 °C under 5% CO₂.

Cytotoxicity study with NaYF₄: Yb³⁺-Er³⁺@Ethane: For cell viability assay, cells were seeded in 96-well plate in 200 µL of their respective culture medium. 24 h after cell growth; cells were treated with different concentrations of nanoparticles and incubated for 3 days. After the incubation time, cells were incubated for 3 h with 0.5 mg mL⁻¹ of MTT (3-(4,5-dimethylthiazol-2-yl)-2,5-diphenyltetrazoliumbromide). Then, the MTT/medium was removed and the precipitated crystals were dissolved in ethanol/DMSO (1:1) solution with shaking for 20 min. The absorbance was measured at 540 nm.

The dose-response curve was plotted as the log concentration (µg mL⁻¹) versus the percentage of cell viability. The mean lethal concentration (LC50) was determined by a non-linear regression equation using GraphPad Prism 5.0 software (San Diego, CA, USA).

Fluorescence imaging of cell uptake of NaYF₄: Yb³⁺-Er³⁺@Ethane: Human breast cancer cells MCF-7 were seeded into a tissue culture chamber with a cover glass bottom in 300 µL of culture medium. Then, the cells were incubated for 24 h with NaYF₄: Yb³⁺-Er³⁺@Ethane at a concentration of 50 µg·mL⁻¹. Fifteen minutes before the end of incubation, cells were loaded with Cell Mask (Invitrogen, Cergy Pontoise, France) for membrane staining at a final concentration of 5 µg mL⁻¹. The cells were washed twice with 1 mL of culture medium. Fluorescence imaging (980 nm excitation wavelength) was performed on living cells with a Carl Zeiss two-photon confocal microscope.

Cellular uptake quantification of NaYF₄: Yb³⁺-Er³⁺@Ethane: The cellular uptake experiment was performed using confocal fluorescence microscopy on living cells. MCF-7 cells were plated on Lab-Tek II Chambered Coverglass (Nunc Ref 155382, Waltham, MA, USA) in a 0.5 mL culture medium for 24 h. Then, cells were treated with concentrations lower than LC50, 25 µg mL⁻¹ and 50 µg mL⁻¹, for 24 h. Control cells were treated with vehicle. Fifteen minutes before the end of incubation, nuclei were stained with Hoechst 33,342 at a final concentration of 5 µg mL⁻¹. Then cells were washed two times with culture medium. Confocal fluorescence microscopy was performed on living cells under a

980 nm wavelength excitation for nanoparticles, 750 nm for nuclei and 522 nm for cell membranes. To calculate the percentage of labeled cells with nanoparticles, cells were counted using the ImageJ program and values obtained were the means of 9 pictures for each concentration.

X-ray computed tomography: X-ray computed tomography images were recorded on the BaLuF₅: Yb³⁺-Er³⁺@Ethane nanoparticles as a powder in a plastic tube showing a transversal image, evidenced that the nanoparticles significantly absorbed the X-ray photons since the image exhibits a suitable contrast. Micro-CT (eXplore CT120; GE HealthCare, Buc, France) examinations were performed using the following parameters: the acquisition consisted of the 720 views acquired, with a 20 ms exposure time per view (Gain: 25 and Offset: 20). The X-ray tube voltage and current were set at 100 kV and 50 mA. CT images were reconstructed using a binning mode of 1 × 1 × 1 and a voxel size of 50 × 50 × 50 μm³. Images were analyzed using MicroView analysis + software (version 2.2, GE Healthcare, Buc, France).

4. Conclusions

In conclusion, we studied the syntheses of core-shell systems with upconversion nanoparticles as their core and with a periodic mesoporous organosilica shell. Depending on the precursor used (bis(triethoxysilyl)ethane or bis(triethoxysilyl)ethylene), the upconversion core nanoparticles were either wrapped with the mesoporous organosilica layer or located on the top of the organosilica nanorods. The NaYF₄: Yb³⁺-Er³⁺@Ethane and BaLuF₅: Yb³⁺-Er³⁺@Ethane nanosystems presented interesting features for theranostics applications such as imaging upon near-infrared or X-ray excitation respectively.

Author Contributions: Conceptualization, A.I.B.N., D.B., and J.-O.D.; methodology, S.R., C.M.J., D.A., N.F., D.G.-M., C.N., and L.M.A.A.; formal analysis, E.O., M.O.; writing—original draft preparation, J.-O.D. and C.C.; writing—review and editing, L.R., D.B.; supervision, R.M., M.G.-B., C.C. and A.I.B.N.

Funding: This research was funded by ANR NanoptPDT. SR thanks the Erasmus Mundus program for a grant.

Acknowledgments: The authors are grateful to Arnaud Briat for CT measurements, and Laure Lichon for technical assistance. This work has been supported by the Spanish Ministry of Science, Innovation and Universities (RTI2018-094426-B-I00).

Conflicts of Interest: The authors declare no conflict of interest.

References

1. Du, X.; Li, X.; Xiong, L.; Zhang, X.; Kleitz, F.; Qiao, S.Z. Mesoporous silica nanoparticles with organo-bridged silsesquioxane framework as innovative platforms for bioimaging and therapeutic agent delivery. *Biomaterials* **2016**, *91*, 90–127. [[CrossRef](#)]
2. Chen, Y.; Shi, J. Chemistry of mesoporous organosilica in nanotechnology: Molecularly organic-inorganic hybridization into frameworks. *Adv. Mater.* **2016**, *28*, 3235–3272. [[CrossRef](#)]
3. Croissant, J.G.; Cattoen, X.; Man, M.W.C.; Durand, J.-O.; Khashab, N.M. Syntheses and applications of periodic mesoporous organosilica nanoparticles. *Nanoscale* **2015**, *7*, 20318–20334. [[CrossRef](#)]
4. Zhu, J.; Niu, Y.; Li, Y.; Gong, Y.; Shi, H.; Huo, Q.; Liu, Y.; Xu, Q. Stimuli-responsive delivery vehicles based on mesoporous silica nanoparticles: Recent advances and challenges. *J. Mater. Chem. B* **2017**, *5*, 1339–1352. [[CrossRef](#)]
5. Castillo, R.R.; Colilla, M.; Vallet-Regi, M. Advances in mesoporous silica-based nanocarriers for co-delivery and combination therapy against cancer. *Expert Opin. Drug Deliv.* **2017**, *14*, 229–243. [[CrossRef](#)] [[PubMed](#)]
6. Pasqua, L.; Leggio, A.; Sisci, D.; Ando, S.; Morelli, C. Mesoporous silica nanoparticles in cancer therapy: Relevance of the targeting function. *Mini-Rev. Med. Chem.* **2016**, *16*, 743–753. [[CrossRef](#)] [[PubMed](#)]
7. Moreira, A.F.; Dias, D.R.; Correia, I.J. Stimuli-responsive mesoporous silica nanoparticles for cancer therapy: A review. *Microporous Mesoporous Mater.* **2016**, *236*, 141–157. [[CrossRef](#)]
8. Croissant, J.G.; Fatieiev, Y.; Almalik, A.; Khashab, N.M. Mesoporous silica and organosilica nanoparticles: Physical chemistry, biosafety, delivery strategies, and biomedical applications. *Adv. Healthc. Mater.* **2018**, *7*, 1700831. [[CrossRef](#)]

9. Croissant, J.G.; Fatieiev, Y.; Khashab, N.M. Degradability and clearance of silicon, organosilica, silsesquioxane, silica mixed oxide, and mesoporous silica nanoparticles. *Adv. Mater.* **2017**, *29*, 1604634. [[CrossRef](#)]
10. Xin, D.; Freddy, K.; Xiaoyu, L.; Hongwei, H.; Xueji, Z.; Shi-Zhang, Q. Disulfide-bridged organosilica frameworks: Designed, synthesis, redox-triggered biodegradation, and nanobiomedical applications. *Adv. Funct. Mater.* **2018**, *28*, 1707325. [[CrossRef](#)]
11. Knezevic, N.Z.; Jimenez, C.M.; Albino, M.; Vukadinovic, A.; Mrakovic, A.; Illes, E.; Janackovic, D.; Durand, J.O.; Sangregorio, C.; Peddis, D. Synthesis and characterization of core-shell magnetic mesoporous silica and organosilica nanostructures. *Mrs Adv.* **2017**, *2*, 1037–1045. [[CrossRef](#)]
12. Rahmani, S.; Chaix, A.; Aggad, D.; Hoang, P.; Moosa, B.; Garcia, M.; Gary-Bobo, M.; Charnay, C.; AlMalik, A.; Durand, J.O.; et al. Degradable gold core-mesoporous organosilica shell nanoparticles for two-photon imaging and gemcitabine monophosphate delivery. *Mol. Syst. Des. Eng.* **2017**, *2*, 380–383. [[CrossRef](#)]
13. Croissant, J.; Salles, D.; Maynadier, M.; Mongin, O.; Hugues, V.; Banchard-Desce, M.; Cattoen, X.; Man, M.W.C.; Gallud, A.; Garcia, M.; et al. Mixed periodic mesoporous organosilica nanoparticles and core-shell systems, application to in vitro two-photon imaging, therapy, and drug delivery. *Chem. Mater.* **2014**, *26*, 7214–7220. [[CrossRef](#)]
14. Mauriello-Jimenez, C.; Knezevic, N.Z.; Rubio, Y.G.; Szunerits, S.; Boukherroub, R.; Teodorescu, F.; Croissant, J.G.; Hocine, O.; Seric, M.; Raehm, L.; et al. Nanodiamond-periodic mesoporous organosilica nanoparticles (pmo) for two-photon photodynamic therapy (pdt) and drug delivery. *J. Mater. Chem. B* **2016**, *4*, 5803–5808. [[CrossRef](#)]
15. Chen, G.Y.; Qju, H.L.; Prasad, P.N.; Chen, X.Y. Upconversion nanoparticles: Design, nanochemistry, and applications in theranostics. *Chem. Rev.* **2014**, *114*, 5161–5214. [[CrossRef](#)]
16. Francolon, N.; Boyer, D.; Leccia, F.; Jouberton, E.; Walter, A.; Bordeianu, C.; Parat, A.; Felder-Flesch, D.; Begin-Colin, S.; Miot-Noirault, E.; et al. Preparation of core/shell $\text{NaYF}_4:\text{Yb},\text{tm}$ @dendrons nanoparticles with enhanced upconversion luminescence for in vivo imaging. *Nanomed.-Nanotechnol. Biol. Med.* **2016**, *12*, 2107–2113. [[CrossRef](#)]
17. Gai, S.L.; Yang, G.X.; Yang, P.P.; He, F.; Lin, J.; Jin, D.Y.; Xing, B.G. Recent advances in functional nanomaterials for light-triggered cancer therapy. *Nano Today* **2018**, *19*, 146–187. [[CrossRef](#)]
18. Ding, B.B.; Shao, S.; Yu, C.; Teng, B.; Wang, M.F.; Cheng, Z.Y.; Wong, K.L.; Ma, P.A.; Lin, J. Large-pore mesoporous-silica-coated upconversion nanoparticles as multifunctional immunoadjuvants with ultrahigh photosensitizer and antigen loading efficiency for improved cancer photodynamic immunotherapy. *Adv. Mater.* **2018**, *30*. [[CrossRef](#)]
19. Gonzalez-Mancebo, D.; Becerro, A.I.; Cantelar, E.; Cusso, F.; Briat, A.; Boyer, D.; Ocana, M. Crystal structure, nir luminescence and x-ray computed tomography of $\text{Nd}^{3+}:\text{Ba}_0.3\text{Lu}_0.7\text{F}_2$ nanospheres. *Dalton Trans.* **2017**, *46*, 6580–6587. [[CrossRef](#)]
20. Zhou, J.; Zhu, X.J.; Chen, M.; Sun, Y.; Li, F.Y. Water-stable NaYF_4 -based upconversion nanophosphors with long-term validity for multimodal lymphatic imaging. *Biomaterials* **2012**, *33*, 6201–6210. [[CrossRef](#)]
21. Croissant, J.; Cattoen, X.; Man, M.W.C.; Gallud, A.; Raehm, L.; Trens, P.; Maynadier, M.; Durand, J.-O. Biodegradable ethylene-bis(propyl)disulfide-based periodic mesoporous organosilica nanorods and nanospheres for efficient in-vitro drug delivery. *Adv. Mater.* **2014**, *26*, 6174–6178. [[CrossRef](#)] [[PubMed](#)]
22. Guan, B.; Cui, Y.; Ren, Z.; Qiao, Z.-A.; Wang, L.; Liu, Y.; Huo, Q. Highly ordered periodic mesoporous organosilica nanoparticles with controllable pore structures. *Nanoscale* **2012**, *4*, 6588–6596. [[CrossRef](#)] [[PubMed](#)]

Sample Availability: Samples of the compounds are not available from the authors.



© 2019 by the authors. Licensee MDPI, Basel, Switzerland. This article is an open access article distributed under the terms and conditions of the Creative Commons Attribution (CC BY) license (<http://creativecommons.org/licenses/by/4.0/>).